HVDC protection criteria for transient stability of AC systems with embedded HVDC links

Juan Carlos Gonzalez, Valentin Costan, Gilney Damm, Abdelkrim Benchaib, Alberto Bertinato, Serge Poullain, Bruno Luscan, Francoise Lamnabhi-Lagarrigue

HVDC protection criteria for transient stability of AC systems with embedded HVDC links

J C Gonzalez* *, V Costan**, G Damm†, A Benchaib*, A Bertinato*, S Poullain*, B Luscan*, F Lamnabhi-Lagarrigue†††

**Supergrid ITE, Villeurbanne, Fr. **EDF Lab Paris-Saclay, Palaiseau, Fr.*
† IBISC Laboratory, Paris-Saclay University, Evry, Fr. †† Laboratoire des signaux et systèmes (LSS), Gif-surYvette, Fr

Keywords: DC faults, Transient stability, AC/DC grids, HVDC grids, HVDC protection.

Abstract

In recent years different protection strategies for High Voltage Direct Current (HVDC) grids have been developed by the industry and academia for the reliable and safe operation of direct current grids. The proposed strategies have different impacts on the AC networks where HVDC grids are connected. In the case of embedded HVDC grids embedded in a synchronous AC network, a partial loss of the HVDC grid might cause the desynchronization of the AC grid. Therefore, it is of utmost importance to assess the impact of those protection strategies into the stability of the whole network. The objective of this paper is to propose a methodology for the transient stability assessment of a simple but representative AC grid in case of DC fault. After validation of the methodology, some HVDC link protection criteria are defined in terms of the Critical Time to Return to Operation (CTRO). These criteria will be helpful for the design of HVDC protection systems, or for the sizing of future HVDC links in order to respect the constraints of the existing protection strategies.

1 Introduction

Since the first High Voltage Direct Current (HVDC) transmission went into service in the 50's, HVDC technologies have been quickly developed. Nowadays, HVDC technologies are mature and rely on a long operational experience. Among the HVDC transmission lines all over the world, a few of them are embedded in AC networks (i.e. HVDC grids with at least two ends being physically connected within a synchronous AC network) [1]. The main reason is the difficult coordination between AC and DC grids. However, due to the growing challenge of network development, the use of embedded HVDC links has been considered more and more.

For years, protection of HVDC grids had been a major hurdle to overcome in the creation of true HVDC grids using Voltage Source Converters (VSC), until the recent proposition of protection devices and schemes [2]. However, in the most severe cases those protection strategies might cause a partial or total interruption of the power flowing through the DC network during a few hundred milliseconds [3]. When an HVDC grid is embedded into an AC grid, this sudden power imbalance might lead to a loss of transient stability (defined in [4]) of the AC grid. For these reasons, it has become imperative to investigate the impact of DC protection strategies on AC grid transient stability. In the literature only a few articles can be found regarding the impact of DC contingencies on the stability of an AC network. In [5] the authors investigate how frequency stability is affected when a contingency in the DC grid occurs. Other articles ([6] and [7]) investigate the impact of a DC fault on the AC transient stability with more detailed models, however those studies are limited to particular cases of DC faults and network topologies. This article aims to contribute to the study of the impact of DC faults on transient stability. The study is made based on simplified models allowing to assess stability as function of different parameters of the system.

The present paper is divided in 4 main sections. First, a modeling technique suitable for analysis of transient stability of AC/DC grids is presented. Then, the technique is applied on a 2-zone mixed AC/DC power system and an extension of the well-known Equal Area Criterion [4] is formulated. In the next section, using Electro-magnetic Transient (EMT) simulation tools, the simplified model is validated. Finally, based on the reduced model, the main factors affecting AC transient stability are listed from which some a priori criteria are proposed for the design of future HVDC grids.

2 AC/DC Power systems modeling for transient stability studies

The dynamics of a mixed AC/DC power system can be described by the set of Differential and Algebraic Equations (DAE)

$$\begin{cases} \dot{\mathbf{x}} = \mathrm{f}(\mathbf{x}, \mathbf{u}, \gamma, \mathrm{t}) \\ 0 = \mathrm{g}(\mathbf{x}, \mathbf{u}, \gamma, \mathrm{t}) \end{cases} \tag{1}$$

where f is the vector of differential equations, g are the algebraic equations, $\mathbf{x}$ are the state variables, γ are the algebraic variables, $\mathbf{u}$ are the input variables and can also be discrete

variables modeling events (i.e. short circuit or line tripping), and t is the time.

For the derivation of the model, consider the multi-machine / multi-converter power system composed of n generators and m HVDC stations interconnected via a transmission network. The converters are considered as complex current sources ($\bar{\mathrm{I}}_{\mathrm{hvdc_k}}$) with independent active power ($\mathrm{P_{hvdc_k}}$) and reactive power ($\mathrm{Q_{hvdc_k}}$, $\forall \mathrm{k} = 1, \dots, \mathrm{m}$) injections.

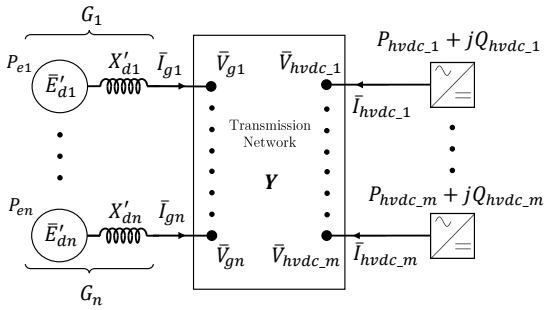

Fig. 1: Multi-machine/multi-converter power system

Synchronous generators are modeled using the classical model of the machine, thus their representation is the association of a complex voltage source representing the internal voltage of the generator ($\bar{\mathrm{E}}'_{\mathrm{di}} = |\mathrm{E}'_{\mathrm{di}}|\mathrm{e}^{\mathrm{j}\delta_{\mathrm{i}}}$) and an inductor representing the transient reactance ($\mathrm{X}'_{\mathrm{di}}$, $\forall \mathrm{i} = 1, \dots, \mathrm{n}$). The voltage $\bar{\mathrm{V}}_{\mathrm{gi}}$ denotes the voltage at the terminals of the $\mathrm{i}-\mathrm{th}$ generator and $\bar{\mathrm{V}}_{\mathrm{hvdc_k}} = |\mathrm{V}_{\mathrm{hvdc_k}}|\mathrm{e}^{\mathrm{j}\theta_{\mathrm{k}}}$ is the voltage at the Point of Common Coupling (PCC) of the $\mathrm{k}-\mathrm{th}$ converter.

The classical model of the machine is used in literature (e.g. [8]) for the study of transient stability of multi-machine systems. Using the classical model for the n generators of the system, and neglecting their damping coefficient, the differential equations representing the first line of Equation 1 are

$$\begin{cases} \dot{\delta}_{\mathrm{i}} = \omega_{\mathrm{i}} \\ \mathrm{M_i}\dot{\omega}_{\mathrm{i}} = \mathrm{P_{mi}} - \mathrm{P_{ei}} \end{cases} \quad \forall \mathrm{i} = 1, \dots, \mathrm{n} \tag{2}$$

where for the $\mathrm{i}-\mathrm{th}$ generator, δ_{i} represents the rotor angle deviation with respect to a synchronous reference, ω_{i} is the rotor speed deviation with respect to the synchronous speed (ω_{s}) , $\mathrm{M_i}$ is the inertia coefficient, $\mathrm{P_{mi}}$ is the mechanical input power, $\mathrm{P_{ei}}$ is the electrical output power. It is important to remark than in the classical model the angle of the internal voltage ($|\mathrm{E}'_{\mathrm{di}}|\mathrm{e}^{\mathrm{j}\delta_{\mathrm{i}}}$) represents also the rotor angle deviation (δ_{i}) of a synchronous generator with one pair of poles.

The set of differential equations described in Equation 2 is related through the electrical output power term ($\mathrm{P_{ei}}$), which is developed in this paper using the internal node representation of the system as proposed in [8]. The algebraic equations of the power system are based on Kirchhoff's law relating currents and voltages in all nodes $\mathbf{I} = \mathbf{Y} \cdot \mathbf{V}$, where $\mathbf{Y}$ is the admittance matrix of the transmission system, $\mathbf{I}$ is the vector of the injected currents, and $\mathbf{V}$ the vector of voltages in every node. Then, matrix $\mathbf{Y}$ is augmented by including the transient reactances of the synchronous generators, nodes with no current injection are eliminated using Kron's reduction, and the resulting matrix is $\mathbf{Y}_{bus}$. The model of the complete network relating voltages and current injections is given by

$$\begin{bmatrix} \mathbf{I}_{\mathrm{g}} \\ \mathbf{I}_{\mathrm{hvdc}} \end{bmatrix} = \overbrace{\begin{bmatrix} \mathbf{Y}_{\mathrm{A}} & \mathbf{Y}_{\mathrm{B}} \\ \mathbf{Y}_{\mathrm{C}} & \mathbf{Y}_{\mathrm{D}} \end{bmatrix}}^{\mathbf{Y}_{\mathrm{bus}}} \begin{bmatrix} \mathbf{E}'_{\mathrm{d}} \\ \mathbf{V}_{\mathrm{hvdc}} \end{bmatrix} \tag{3}$$

where $\mathbf{Y}_{\mathrm{A}}$,$\mathbf{Y}_{\mathrm{B}}$, $\mathbf{Y}_{\mathrm{C}}$ and $\mathbf{Y}_{\mathrm{D}}$ are submatrices of dimensions $(\mathrm{n} \times \mathrm{n})$, $(\mathrm{n} \times \mathrm{m})$, $(\mathrm{m} \times \mathrm{n})$ and $(\mathrm{n} \times \mathrm{m})$ respectively. $\mathbf{I}_{\mathrm{g}}$ and $\mathbf{E}'_{\mathrm{d}}$ are respectively the vectors containing the injected current and internal voltage of generators. $\mathbf{I}_{\mathrm{hvdc}}$ and $\mathbf{V}_{\mathrm{hvdc}}$ are the injected currents and voltages at AC bus-bars of the converters (see [9] for more details on this formulation). This linear equation can be solved in order to obtain the generator's currents as a function of the voltages of the system and the injected current by the HVDC systems. The solution is given by

$$\mathbf{I}_g = \mathbf{Y}_{SN}\mathbf{E'}_d + \mathbf{K}_{hvdc}\mathbf{I}_{hvdc} \tag{4}$$

with $\mathbf{Y}_{\mathrm{SN}} = (\mathbf{Y}_{\mathrm{A}} - \mathbf{Y}_{\mathrm{B}}\mathbf{Y}_{\mathrm{B}}\mathbf{Y}_{\mathrm{C}})$ and $\mathbf{K}_{\mathrm{hvdc}} = \mathbf{Y}_{\mathrm{B}}\mathbf{Y}_{\mathrm{D}}^{-1}$. Matrix $\mathbf{Y}_{\mathrm{SN}}$ is the admittance matrix relating all generators voltages and currents, and $\mathbf{K}_{\mathrm{hvdc}}$ describes the effect of HVDC injected currents into the generator currents. Note that elements in matrix $\mathbf{K}_{\mathrm{hvdc}}$ are dimensionless. Elements of $\mathbf{Y}_{\mathrm{SN}}$ and $\mathbf{K}_{\mathrm{hvdc}}$ can be expressed in complex form as follows

$$\bar{\mathrm{Y}}_{\mathrm{SN_{ij}}} = \mathrm{G_{ij}} + \mathrm{jB_{ij}} \quad \text{and} \quad \bar{\mathrm{K}}_{\mathrm{hvdc_{ik}}} = \mathrm{D_{ik}} + \mathrm{jF_{ik}} \tag{5}$$

$\mathrm{G_{ij}}$ and $\mathrm{B_{ij}}$ are the equivalent conductance and susceptance between generators buses i and j. $\mathrm{D_{ik}}$ and $\mathrm{F_{ik}}$ are the real and imaginary parts of the element $\mathrm{K_{hvdc_{ik}}}$ which denote the effect of the injected current of the $\mathrm{k}-\mathrm{th}$ converter on the current injected by the $\mathrm{i}-\mathrm{th}$ generator. Then, the expression of the active power supplied by the $\mathrm{i}-\mathrm{th}$ machine ($\mathrm{P_{ei}}$) in Equation 2, which is given by

$$\mathrm{P_{ei}} = \Re[\bar{\mathrm{E}}'_{\mathrm{di}}\bar{\mathrm{I}}^{*}_{\mathrm{gi}}] \tag{6}$$

The substitution of 4 into Equation 6 yields

$$\mathrm{P_{ei}} = \Re\left[\bar{\mathrm{E}}'_{\mathrm{di}}\sum_{\mathrm{j=1}}^{\mathrm{n}}\bar{\mathrm{Y}}^{*}_{\mathrm{SN_{ij}}}\bar{\mathrm{E}}'^{*}_{\mathrm{dj}} - \bar{\mathrm{E}}'_{\mathrm{di}}\sum_{\mathrm{k=1}}^{\mathrm{m}}\bar{\mathrm{K}}^{*}_{\mathrm{hvdc_{ik}}}\bar{\mathrm{I}}^{*}_{\mathrm{hvdc_k}}\right] \tag{7}$$

The conjugate of the complex current injected by the $\mathrm{k}-\mathrm{th}$ converter is given by

$$\bar{\mathrm{I}}^{*}_{\mathrm{hvdc_k}} = \frac{\mathrm{P_{hvdc_k}} + \mathrm{jQ_{hvdc_k}}}{|\mathrm{V_{hvdc}}|\mathrm{e}^{\mathrm{j}\theta_{\mathrm{k}}}} \tag{8}$$

Substituting Equations 8 and 5 into Equation 7, the electric power supplied by the $\mathrm{i}-\mathrm{th}$ generator is derived as

$$\begin{aligned} \mathrm{P_{ei}} = &\sum_{\mathrm{j=1}}^{\mathrm{n}}|\mathrm{E}'_{\mathrm{di}}||\mathrm{E}'_{\mathrm{dj}}|(\mathrm{G_{ij}}\cos\delta_{\mathrm{ij}} + \mathrm{B_{ij}}\sin\delta_{\mathrm{ij}}) \\ &+ \Re\left[\sum_{\mathrm{k=1}}^{\mathrm{m}}\frac{\bar{\mathrm{E}}'_{\mathrm{di}}}{\bar{\mathrm{V}}_{\mathrm{hvdc_k}}}(\mathrm{D_{ik}} + \mathrm{jF_{ik}})(\mathrm{P_{hvdc_k}} + \mathrm{jQ_{hvdc_k}})\right] \end{aligned} \tag{9}$$

with $\delta_{ij} = \delta_i - \delta_j$.

Considering that the HVDC converters have a constant power characteristic, their power injections are the same regardless the angles of the internal voltages of the machines. Therefore, the complex ratio of voltages ($\bar{E}'_{di}/\bar{V}_{hvdc_k}$) can be assumed constant and equal to its steady state value. With this assumption Equation 9 becomes

$$\begin{aligned} P_{ei} = &\sum_{j=1}^{n} |E'_{di}||E'_{dj}|(G_{ij}\cos\delta_{ij} + B_{ij}\sin\delta_{ij}) \\ &+ \sum_{k=1}^{m} a_{ik}^{dc}\, P_{hvdc_k} - \sum_{k=1}^{m} b_{ik}^{dc}\, Q_{hvdc_k} \end{aligned} \tag{10}$$

In the case of the loads, they can be taken into account by representing them by constant power loads and using the same equations as in the case of the power injections of the HVDC link.

3 Transient stability of a 2-machines AC/DC system

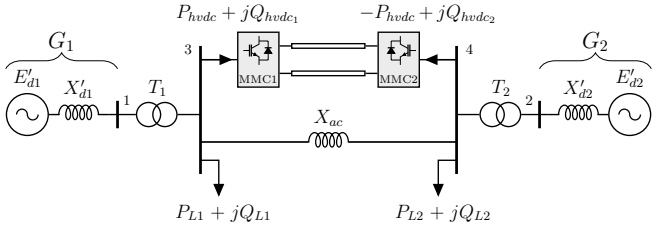

Fig. 2: 2-Area 2-Machine AC/DC power system

In this section the methodology is applied on a 2-area system connected through an hybrid transmission system composed of a loss-less AC line (with reactance X_{ac}) in parallel with an HVDC system as shown in Figure 2. Each area is composed of a synchronous generator (G_1 and G_2) connected to a step-up transformer (T_1 and T_2) and supplies power to a local load ($P_1 + jQ_1$ and $P_2 + jQ_2$). The 2-area AC/DC system has been chosen since every generator can represent an aggregated region of generators. Also the HVDC link can represent a multi-terminal DC grid with two ends connected to the AC grid.

After reducing the nodal matrix equation for finding the currents injected by each machine, for the system in Figure 2, Equation 4 becomes

$$\begin{aligned} \begin{bmatrix} \bar{I}_{g1} \\ \bar{I}_{g2} \end{bmatrix} = &\overbrace{\begin{bmatrix} \frac{1}{jX_{eq}} & -\frac{1}{jX_{eq}} \\ -\frac{1}{jX_{eq}} & \frac{1}{jX_{eq}} \end{bmatrix}}^{\mathbf{Y}_{SN}} \begin{bmatrix} \bar{E}'_{d1} \\ \bar{E}'_{d2} \end{bmatrix} \\ &- \overbrace{\begin{bmatrix} \frac{X_{T2}+X_{ac}+X'_{d2}}{X_{eq}} & \frac{X_{T2}+X'_{d2}}{X_{eq}} \\ \frac{X_{T1}+X'_{d1}}{X_{eq}} & \frac{X_{T1}+X_{ac}+X'_{d1}}{X_{eq}} \end{bmatrix}}^{\mathbf{K}_{hvdc}} \begin{bmatrix} \bar{I}_3 \\ \bar{I}_4 \end{bmatrix} \end{aligned} \tag{11}$$

with $X_{eq} = X_{T1} + X_{T2} + X_{ac} + X'_{d1} + X'_{d2}$, where X_{T1} and X_{T2} are the equivalent reactances of the transformers. $\bar{I}_3$ and $\bar{I}_4$ are the complex currents injected in buses 3 and 4 respectively. In this particular case the loads and the converters are connected to the same buses, thus $\bar{I}_3$ and $\bar{I}_4$ depend on the loads and the power injections of the HVDC link following the relation given by Equation 8. Using Equation 10, the electrical output power term of each generator can be derived. Then the dynamic equations of the system are written as follows

$$\begin{cases} M_1\ddot{\delta_1} = P_{m1} - \frac{|E'_{d1}||E'_{d2}|}{X_{eq}}\sin(\delta_1 - \delta_2) - P_1^{dc} - P_1^{L} \\ M_2\ddot{\delta_2} = P_{m2} - \frac{|E'_{d1}||E'_{d2}|}{X_{eq}}\sin(\delta_2 - \delta_1) - P_2^{dc} - P_2^{L} \end{cases} \tag{12}$$

Where P_1^{dc} and P_2^{dc} represent the effect of the complex power injections of all the converters into generators 1 and 2 respectively (i.e. they correspond to the second line of Equation 10). Similarly, P_1^{L} and P_2^{L} describe the effect of all the complex loads into generators 1 and 2 respectively.

Making $\delta = \delta_1 - \delta_2$ in Equation 12, an equivalent AC/DC single-machine machine infinite bus (AC/DC SMIB) system can be derived. This system is composed of an equivalent machine connected to a fictitious infinite bus via an AC transmission line in parallel with an HVDC link. The equation describing its behavior is given by

$$M\ddot{\delta} = P_m - [\overbrace{P_L + P_{dc}}^{P_c} + P_{max}\sin(\delta)] = P_m - P_e \tag{13}$$

with an equivalent inertia of value

$$M = M_1M_2/(M_1 + M_2) \tag{14}$$

The equivalent mechanical power is given by

$$P_m = \frac{M_2P_{m1} - M_1P_{m2}}{M_1 + M_2} \tag{15}$$

and the constant component P_c of the equivalent output power P_e is given by the sum of terms

$$P_L = \frac{M_2P_1^{L} - M_1P_2^{L}}{M_1 + M_2} \text{ and } P_{dc} = \frac{M_2P_1^{dc} - M_1P_2^{dc}}{M_1 + M_2} \tag{16}$$

The component of the output power due to the AC network is given by

$$P_{max} = \frac{|E'_{d1}||E'_{d2}|}{X_{eq}} \tag{17}$$

3.1 AC/DC Equal area criterion

Transient stability of system described by Equation 13 can be assessed using the AC/DC Equal Area Criterion (AC/DC EAC) presented in Figure 3 where the $P - \delta$ curves are plotted. In case of DC fault, three main operating conditions are adopted: pre-fault (O), fault (D_i), post-fault (P) conditions.

Pre-fault operating condition: it corresponds to the power system operating at some stable steady-state condition before

the occurrence of the fault. In this state the electric power is noted $\mathrm{P_e^0}$ in Figure 3. The HVDC link reactive and active power injections are included in the term noted $\mathrm{P_c^0}$.

Fault operating conditions: depending on the protection strategy, many fault operating conditions between fault occurrence and the DC power restoring can take place. The behavior of each faulted operating condition is described by its reactive and active power injections. The electric power is denoted $\mathrm{P_e^{Di}}$ for $\mathrm{i} = 1...\mathrm{q}$ where q is the number of faulted operating conditions given by the adopted protection strategy. Similarly, the power injections are noted $\mathrm{P_c^{Di}}$ for $\mathrm{i} = 1...\mathrm{q}$. In Figure 3 only one fault operating condition is represented.

Post-fault operating condition: it corresponds to the operating condition when the protection sequence is completed. In this operating condition $\mathrm{P_e} = \mathrm{P_e^P}$ and $\mathrm{P_c} = \mathrm{P_c^P}$. If the fault is managed to be isolated and the power transmitted via the HVDC link is totally restored, then the post-fault state is equal to the pre-fault state $\mathrm{P_e^P} = \mathrm{P_e^0}$. If the fault is permanent, the post fault state is equal to one of the faulted states depending on the strategy used $\mathrm{P_e^P} = \mathrm{P_e^{Di}}$.

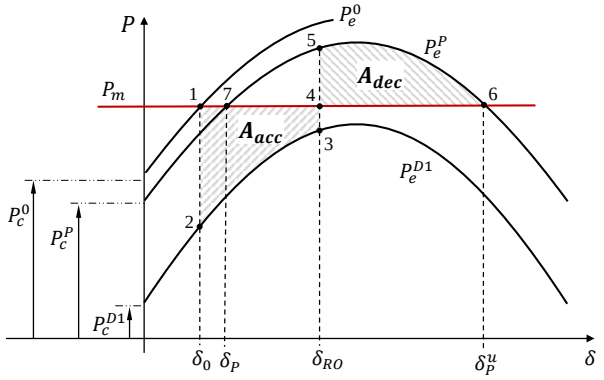

Fig. 3: AC/DC Equal area criterion in case of DC fault

In the pre-fault condition, the system works in steady state operation at point 1 where the rotor angle is equal to δ_0. When the fault occurs, power of the HVDC is lost and the electrical power goes from point 1 to 2. The assumption made here is that fault detection and fault current interruption are fast enough so the fault current has no impact on transient stability. At point 2, the accelerating power is positive and the rotor accelerates. Its acceleration is positive until the protection sequence is complete an the HVDC returns to operation. When the HVDC power is restored the electrical power of the generator goes from point 3 to 5. At this point the angle has reached the value δ_{RO}. At point 5 the rotor starts to decelerate but its speed is still positive so the angle δ continues to increase. If angle δ exceeds the critical angle δ_P^u stability is lost. In the other hand, if the rotor speed goes from positive to negative before the angle δ reaches δ_P^u stability is maintained. If stability is maintained the system will oscillate around point 7. As in its conventional version the AC/DC EAC states that if the available deceleration area $\mathrm{A_{dec}}$ is bigger than the acceleration area $\mathrm{A_{acc}}$ the system remains stable, otherwise stability will be lost.

4 Validation of the AC/DC Equal Area Criterion

In this section the simplified model of the AC/DC system described by Equation 13 is validated by comparing its behavior to the one of a detailed model using the Electromagnetic Transient Simulation software EMTP-RV®.

The HVDC link of the simulated system is an MMC-based HVDC link in bipolar configuration. The protection strategy known as the Converter-Breaker non-selective strategy and presented in [10] and [11] is used. Generators are modeled using its third-order model with constant mechanical input power $\mathrm{P_m}$ and constant excitation $\mathrm{E_{fd}}$. The controls of the electrical generator are not simulated in order to obtain an undamped response as in the simplified swing equation. The generator mechanical input is set to 0.66 pu. The MMC active power reference is set to 0.44 pu thus the power flowing through the parallel AC line is 0.22 pu. The reactive power references of the HVDC link are set to zero. The base power correspond to the nominal power of the generators (900 MVA)

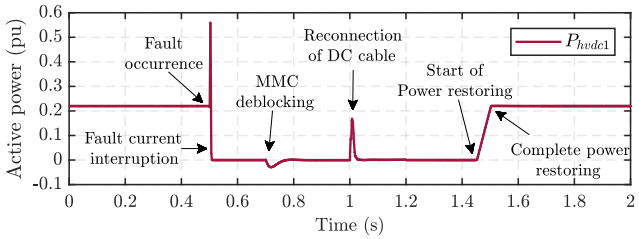

Fig. 4: AC side power injections of the faulted pole of station 1 during a DC fault using the Converter-Breaker strategy

The power injection of an MMC converter of station 1 during a pole-to-earth DC fault is shown in Figure 4. In steady state operation the power flowing through the pole is set to 0.22 pu. When the fault occurs, the current flowing through the station increases until the fault is detected and the DC circuit breakers disconnect the faulted cable. The use of IGBT transistors connected in anti-parallel to the diodes allows the MMC to force the fault current pass through the diodes impeding the capacitors from contributing to the fault current. This action is known as "converter blocking". When the faulted cable is isolated the MMC can be deblocked. Once the fault has been cleared, the cable can be reconnected and the control of the DC side voltage is recovered. Then, the system is ready to return to operation and power is smoothly restored to its initial value.

The detailed model is compared with the numerical solution of equation 13 using Matlab®. In order to perform the numerical solution, coefficients in Equations 13 are calculated at the pre-fault state using the results of a power flow analysis. The computing of those coefficients allows to calculate the terms in the faulted and post-fault state. The comparison is presented in Figure 5, where it can be seen that the transient behavior of two models is similar. Minimal differences can be observed. This is caused mainly because the variation of the voltages are not taken into account in the simplified model.

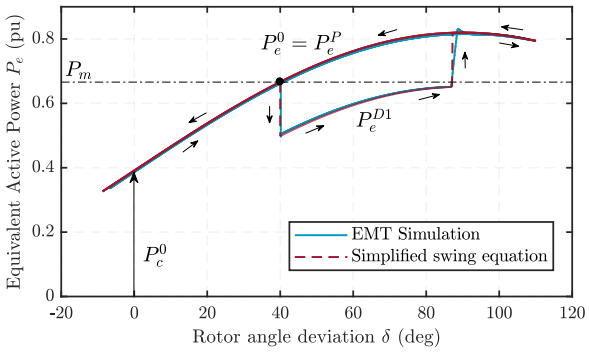

Fig. 5: Validation of AC/DC Equal area criterion

5 Protection criteria for AC/DC systems

In order to derive normalized criteria, the reduced model in equation 13 must be expressed in per unit. With this aim in mind, the mechanical power as well as the loads of the systems, assumed to remain invariant, can be regrouped by introducing $\mathrm{P_{SL}} = \mathrm{P_m} - \mathrm{P_L}$. $\mathrm{P_{SL}}$ is chosen as the base power of the system. Equation 13 takes the following form:

$$\frac{2\mathrm{H}}{\omega_\mathrm{s}}\ddot{\delta} = 1 - \mathrm{P_{dc}} - \mathrm{P_{max}}\sin(\delta) \quad \mathrm{pu} \tag{18}$$

where $\mathrm{H} = \omega_\mathrm{s}\mathrm{M}/2\mathrm{P_{SL}}$ is an aggregated inertia constant in seconds. The advantage of such formulation is that the equivalent exchanged power between the equivalent machine and the fictitious infinite bus is equal to 1pu.

While in conventional AC systems the Critical Clearing Time (CCT) is used to quantify transient stability margins, in this article it is proposed to used the term Critical Time to Return to Operation (CTRO) in case of DC contingencies. The CTRO is the maximum time during which the HVDC active power can be interrupted without the system losing its stability. Based on Equation 18, in can be concluded that the CRTO depends mainly in the following factors:

- The aggregated inertia of both regions (H)
- The equivalent ratio between the power transmitted by the HVDC and the total power exchanged between two regions ($\mathrm{P_{dc}}/(\mathrm{P_{dc}} + \mathrm{P_{max}}\sin\delta_0)$)
- The amount of DC power lost during the fault
- The different fault operating conditions determined by the protection strategy and the nature of the fault
- The reactive power injections of HVDC stations during fault treatment and restoration
- The angle difference δ_0 between both regions in the pre-fault state
- The amount of power restored after return to operation (post-fault)

In a first example, by iterative simulations, the CTRO is calculated as function of the aggregated inertia and the equivalent ratio between the HVDC power and the total power exchanged ($\mathrm{P_{dc}}/(\mathrm{P_{dc}} + \mathrm{P_{max}}\sin\delta_0)$). Commonly, to avoid system stability problems, the angular difference across a transmission line is rarely allowed to exceed about 40 degrees; typically, angle differences are less than 20 to 30 degrees. For the results shown in Figure 6 the initial angle between machines δ_0 is set to 30 degrees. In order to simplify the analysis, reactive power injections are assumed to be zero for all cases. In the results depicted in Figure 6a the CRTO is calculated for a loss of 100% of the HVDC power which is the case of a pole-to-pole short circuit in a monopolar HVDC link. In Figure 6b the CRTO is plotted for a loss of 50% of the HVDC transmitted power. This case corresponds to a pole to ground fault in a bipolar HVDC link as depicted in Section 4.

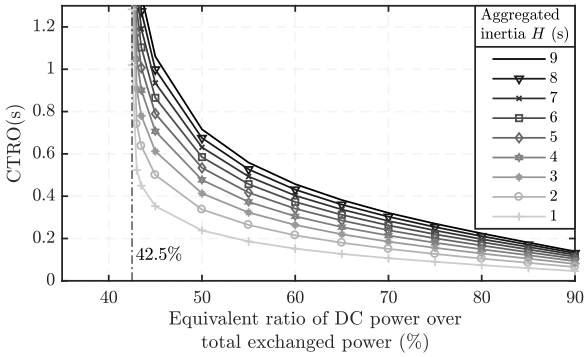

(a) 100% of the HVDC power is lost (Monopolar configuration)

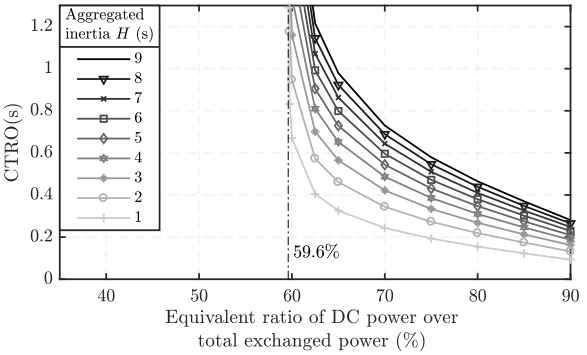

(b) 50% of the HVDC power is lost (Bipolar configuration)

Fig. 6: CRTO as function of the aggregated inertia H and the ratio of HVDC transmitted power over the total exchanged power between regions. $\delta_0 = 30°$

From the results it can be seen that transient stability margins decrease when the aggregated inertia of the system is lower. In [10] it is stated that the protection strategy used in this paper takes around 180ms for a complete restoration of the active power after the fault occurrence. It can be observed that for a CTRO of 180ms, transient stability is at stake only if the HVDC link transfers an important amount of power compared to the parallel AC group (e.g 65% for an aggregated inertia of 2s in case of a 100% $\mathrm{P_{dc}}$ loss).

It must be also noticed that for lower ratio of DC power over total exchanged power, no CTRO is found. This means that the active power can be lost permanently without the system losing stability. Results show that there is a threshold value of the power ratio before which the system remains stable regardless the aggregated inertia. For the case of Figure 6a, this value is 42.5% whereas for the case in Figure 6b the threshold ratio is 59.6%.

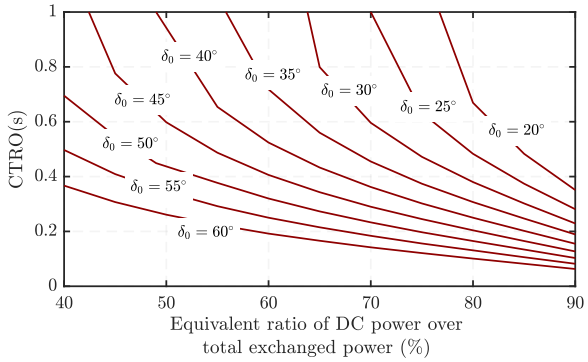

Fig. 7: CRTO as function of the initial angle δ_0 and the ratio of HVDC transmitted power over the total exchanged power between regions. Complete loss of the HVDC power and $H = 6s$

In Figure 7 the impact of the initial angle deviation on the CRTO is illustrated. In this example it is assumed a complete loss of the HVDC power and an inertia of 6s. Higher values of the initial angle denote a more stressed grid, thus lower transient stability margins. It can be seen that for higher values of the initial angle the CRTO is lower, while for normal operation angles (between $20°$ and $30°$) CTRO values barely reach 200ms for very high HVDC power ratios.

6 Conclusions

A methodology for the assessment of transient stability in case of DC faults was presented. Based on the classical model of the machine and the current injection model of the HVDC converters, an AC/DC equal area criterion for a two-area system was presented. If the behavior of the HVDC link in its fault operating conditions is known, transient stability can be assessed using the proposed AC/DC EAC. Since the methodology presented is based on simple models, parametric studies of the transient stability margins can be more easily performed. The AC/DC EAC method is suitable to be used in future works for the comparison of different HVDC protection strategies

Through this analysis it was also possible to identify the main parameters influencing AC/DC the transient stability. It is concluded that transient stability risks to be lost when the AC regions are interconnected by a weak AC transmission systems. Transient stability margins are decreased also when the power flowing through the HVDC link is high compared to the power in the AC parallel transmission group. Even if the models used in this work are simplified, the results can give a priori criteria for the design of future embedded HVDC grids.

Acknowledgements

This research work was held at the SuperGrid Institute funded by the French National Research Agency

References

[1] S. Henry, O. Despouys, R. Adapa, L. Barthold, C. Bayfield, K. Bell, J.-L. Binard, A. Edris, P. Egrot, W. Hung *et al.*, "Influence of embedded hvdc transmission on system security and ac network performance," *Electra*, no. 267, pp. 79–86, 2013.

[2] M. J. Carrizosa, J. Cortes, A. Benchaib, P. Alou, G. Damm, J. Cobos, and F. Lamnabhi-Lagarrigue, "Dc/dc converters as dc circuit-breakers in hvdc networks operation," in *Power Electronics and Applications (EPE'14-ECCE Europe), 2014 16th European Conference on*. IEEE, 2014, pp. 1–10.

[3] W. Leterme and D. Van Hertem, "Classification of fault clearing strategies for hvdc grids," 2015.

[4] P. Kundur, *Power System Stability and Control*. McGraw-Hill Education (India), 1994.

[5] M. Abedrabbo, M. Wang, P. Tielens, F. Z. Dejene, W. Leterme, J. Beerten, and D. Van Hertem, "Impact of dc grid contingencies on ac system stability," 2017.

[6] G. Li, J. Liang, C. E. Ugalde-Loo, P. Coventry, and J. Rimez, "Dynamic interactions of dc and ac grids subject to dc faults," in *Power Electronics and Motion Control Conference (IPEMC-ECCE Asia), 2016 IEEE 8th International*. IEEE, 2016, pp. 2627–2633.

[7] G. Tang, Z. Xu, and Y. Zhou, "Impacts of three mmc-hvdc configurations on ac system stability under dc line faults," *IEEE Transactions on Power Systems*, vol. 29, no. 6, pp. 3030–3040, 2014.

[8] A. Pai, *Energy function analysis for power system stability*. Springer Science & Business Media, 2012.

[9] M. Pai, K. Padiyar, and C. Radhakrishna, "Transient stability analysis of multi-machine ac/dc power systems via energy-function method," *IEEE Transactions on Power Apparatus and Systems*, no. 12, pp. 5027–5035, 1981.

[10] D. Loume, A. Bertinato, B. Raison, and B. Luscan, "A multi-vendor protection strategy for hvdc grids based on low-speed dc circuit breakers," 2017.

[11] W. Leterme and D. Van Hertem, "Deliverable 4.2: Broad comparison of fault clearing strategies for dc grids," PROgress on Meshed HVDC Offshore Transmission Networks (PROMOTioN), Tech. Rep., 2017.